Postprint of: Bień A., Szkodo M., Surface treatment of C80U steel by long CO_2 laser pulses, Journal of Materials Processing Technology, Vol. 217 (2015), pp. 114-121, DOI: 10.1016/j.jmatprotec.2014.11.001

Surface treatment of C80U steel by long CO_2 laser pulses

Anna Bień[a], Marek Szkodo[b,*]

a Technical Sciences Faculty, University of Warmia and Mazury in Olsztyn, Oczapowskiego 11, 10-719 Olsztyn, Poland

b Mechanical Engineering Faculty, Gdansk University of Technology, Narutowicza 11/12, 80-233 Gdansk, Poland

a b s t r a c t

The paper presents the results of laser-melted C80U steel. The processed steel was placed between two permanent magnets and laser beam whose scanning velocity was 10 mm/s. CO_2 laser beam was working in pulse mode. Pulses were generated at 100% of the average preset power of 700 W, with 45 ms irradiation, zero interval between pulses and beginning of pulse repetition upon the achievement of the average laser power. During the operation, the laser beam generated plasma. The cyclic process of plasma generation induced by long laser pulses was validated experimentally with the use of a high-speed camera. Calculated speed of the plasma propagation velocity was 5.255 × 102cm/s. The melted path had characteristic “folds”, and it comprised of a series of overlapping melted areas. The distance between adjacent “folds” correlated with beam displacement velocity which indicates that plasma plumes were generated cyclically at the beginning of the generation of successive laser pulses. Hardness test of the processed steel revealed that surface irregularities were caused by mechanical effects of pulsed plasma. The hardness of the analyzed C80U steel varied significantly between areas of measurement. In selected measurement points, hardness values reached 3200–3100 HV, 1800 HV and 400–300 HV. XRD and SAD investigation revealed in microstructure of processed steel martensite, partially dissolved cementite $(FeCrMn)_3C$ and small amount of retained austenite. The microstructure revealed by TEM indicates that in areas with greater hardness there were higher dislocations and twins density. Hardness test with a multiple load cycle with increasing load from 0.5 N to 20 N showed that shock waves formed as a result of plasma plume propagation interacting with the melted steel, thus contributing to the strain hardening of processed steel and providing an occurrence of the biggest residual stresses near the surface and reducing them with the depth of melted steel. Impact stress generated by extending plasma also facilitated the phase transformation of austenite and thus reduced the amount of retained austenite.

1. Introduction

Laser surface treatment is a relatively new and promising pro-cess for enhancing the surface properties of a component. Laser treatment is used mainly to increase the durability of tools and machine parts through the implementation of the following technology groups: with or without melting of the surface of the workpiece, and with surface desiccation of processed alloy. Laser treatment with melting the surface of treated alloy include laser alloying, laser cladding and laser surface melting (LSM). Thanks to laser surface melting, the top layer of the steel can get fine-grained microstructure and partial or complete dissolution in the phases in the form of oxides or carbides. Rapid crystallization ensures that after dissolution they do not precipitate again or separate from a solid solution in a different form. The laser treatment allows solid solutions to become strongly saturated. Therefore, laser melting is accompanied by a strong fragmentation and dispersion phase and purification of grain boundaries. Laser beam melting and subsequent rapid cooling leads also, as a rule, to the creation of the state of

residual stress within the processed material due to diffusion retarding (Gireń et al., 1999). The degree of enhancement of mechanical properties of laser processed steel depends on the final microstructure formed. Szkodo(2005) reported that cavitation erosion resistance of C45 steel depends on the type of microstructure obtained by laser surface treatment. Yasavola et al. (2013) in turn, reported that increase of the laser energy and reduction of the laser scanning rate results in deeper melt pool formation. Moreover, laser plasma melting has led to the complete dissolution of the carbides and re-solidification of cellular/dendritic structure of a fine scale surrounded by a continuous interdendritic network. This caused an increase in surface microhardness, 2–4 times over that of the base metal. Kac and Kusinski (2004) indicated that the high chemical homogeneity and fine structure of the melted zone in ASP2060 steel were attributed to high cooling rates due to the short interaction time with the Nd:YAG pulsed laser radiation and relatively small volume of the melted material. An increase in microhardness of the laser-melted zone after tempering may be probably attributed to fine precipitates formed in melted zone and to the transformation of the retained austenite. Samples treated by a pulsed laser radiation showed better wear resistance than the conventionally heat-treated ones. Jiang et al. (2011) studied the effects of various laser processing parameters, including laser pulse energy, pulse duration and defocus distance, on characteristics of the laser treated AISI O1 tool steel. Results of their investigations show that the maximum diameter and depth of transformation hardening zones with no surface melting increased with the increase of laser pulse energy. However, they are not markedly affected by laser pulse duration. On the other hand, longer pulse durations at a given pulse energy reduce the size of the softening zone surrounding the central hardening zone and are thus more favorable for the most practical applications. Short laser pulse durations below 8 ms tend to produce shallower hardening zones and are not recommended for wear applications. Nath et al. (2012) investigated the effects of various process parameters, viz. laser power, beam diameter, scan speed, pulse duration, repetition frequency and duty cycle on the surface transformation hardening during laser processing of AISI 1055 steel. The study shows that the soaking time of the top surface layer at a temperature above the phase transformation temperature, on which the homogeneity of microstructure and the depth of hardening depend, can be increased by repetitive laser pulse heating in comparison to continuous wave laser heating. The depth of hardness increases with the number of incident laser pulses at low frequencies in the range of Hz. Telasang et al. (2014) investigated structure–property correlation in laser surface treated AISI H13 tool steel for improved mechanical properties. They reported that depth of the hardened or melted layer of the surface increases with the increase of the incident laser energy density. Surface melting occurs at a higher laser energy density (>75 J/mm^2) and leads to the formation of inhomogeneous microstructure comprising non-uniform distribution of retained austenite, carbides (along inter-dendritic boundary) and martensite with the irrespective volume fractions varying with depth. Application of intermediate laser energy density (50–75 J/mm^2) yields a hardened layer with dispersion of ultrafine mixed carbides ($M_{23}C_6$, M_7C_3, MCorM_2C). Laser treatment with a very low laser energy density (<50 J/mm^2) leads to formation of an over-tempered microstructure consisting of low carbon martensite and coarse carbide precipitates. Micro-tensile studies with specially machined samples from the surface melted zone following LSM with the laser energy density of 100 J/mm^2 records a high yield strength of 1310 MPa along with poor ductility, marked by brittle failure. On the other hand, a similar sample from laser surface hardened zone treated with the laser energy density of 62.5 J/mm^2 yielded even higher yield strength of 1460 MPa with a maximum elongation of 3.6%. Though both laser surface hardening (LSH) and laser surface melting (LSM) produced higher yield strength compared to hardened and tempered AISI H13 tool steel, LSH yielded a combination of higher elongation (3.6%), than that after LSM (0.97%), with high yield strength and hence was considered a better option. Breczko and Bień (2006) reported that an increase in the surface smoothness and microstructures responsible for high hardness of the 50H grade steel which was multiple melted using a laser beam were achieved due to appropriate combination of treatment

parameters. Bien and Szachnowski (1996) in turn found relationship between laser parameters of melted 21H12NMFA martensitic steel and the degree of homogeneity of the microstructure of treated steel. Dutta Majumdar et al. (2003) tried to enhance pitting corrosion resistance and microhardness of a commercial Mg alloy, MEZ(Zn 0.5%, Mn 0.1%, Zr 0.1%, rare earth elements 2%, Mg remaining percentage) by laser surface melting. Microhardness of the laser surface melted layer was improved to 85–100 VHN as compared to 35 VHN of the as-received MEZ. Pitting corrosion resistance of the laser surface melted MEZ, significantly improved in a 3.56 wt. % NaCl solution because of grain refinement and redistribution of the intermetallic phases following rapid quenching associated with the process. The wear resistance of laser surface melted layer was also improved as compared to as-received MEZ. Also Basu et al. (2008) developed an amorphous coating with Fe48Cr15Mo14Y2C15B6 bulk metallic glass on AISI 4140 substrate by laser surface processing. The microhardness of the coated layer was significantly improved to as high as 950 VHN as compared to240 VHN of the substrate. A significant improvement in wear resistance was achieved due to laser surface coating. Residual stress developed in the coated layer was much lower than that of the as received substrate but compressive in nature. In certain circumstances of the laser melting, optical discharge plasma may be created, which can alter the effects of this treatment (Gireń et al., 1999). Irradiation intensity, wavelength and pulse duration are the key parameters that determine plasma formation during laser processing. The experiment described in this paper was designed to investigate the type of side effects which accompany laser irradiation when the time of pulse duration, the number of repetitions and the initial generation energy (starting at zero or at a specified stable level) are modified. The paper discusses the results of C80U steel sample melting by an optical discharge plasma which was generated by a series of long CO_2 laser pulses.

2. Experimental procedure

Sample for investigations in semi-spherical shape (radius 13 mm, thickness 8 mm) was made of C80U steel. C80U steel sample has been subjected to normalizing. Chemical composition of C80U steel and heat treatment parameters are presented in Table 1. Subsequent prepared sample was superficially

Table 1
Chemical composition of C80U steel and its heat treatment parameters.

Chemical composition (mass %)								Heat treatment	Hardness after normalizing [HV]
C	Mn	Si	P max	S max	Cr max	Ni max	Cu max	Normalizing [°C]	
0.8	0.25	0.2	<0.025	<0.025	0.15	0.2	0.2	760	240

processed by laser beam. A continuous-wave/pulsed 1750 W Wegmann Baasel carbon dioxide laser was used to generate laser pulses with various length of the pulses, different number of repetitions and various levels of initial generation energy – starting at zero or at a specific power level. This paper discusses the results of program 8 where pulses were generated at 100% of the average preset power of 700 W, with 45 ms length of the pulses, zero interval between pulses and beginning of pulse repetition upon the achievement of average laser power. The buffer gas was argon which was applied at pressure slightly higher than atmospheric pressure. The power control indicator was set at 360 mA.

Beam scanning velocity was 10 mm/s. The sample was placed between two permanent magnets on a metal platform measuring 25 mm × 40 mm × 80 mm. The sample was processed at the distance of 117 mm between the converging lens and the processed surface. A zinc selenite lens with 3.8 in. focal length was used to converge the beam with the diameter of 18 mm. Spot size was 1.9096 mm. Fast camera recorded the images during the laser processing. The images were acquired when beam generation energy was stabilized. Photographs were taken at intervals of 0.222 ms. The camera was set at 4500 frames per second. An electron microscope (TEM) was used for visualization of microstructures in the plane normal to the processing path. Preparation of the cross-section samples for transmission electron microscopy was performed in the following steps. First slice of 2 mm width and 6 mm length was cut out of the laser beam processed path using a diamond wire saw. Next the slice was embedded in the tube with an outer diameter of 3 mm and an inner diameter of ca. 2.12 mm with the two-component epoxy glue. Then the tube was glued onto the Al holder with thermo-wax and disks of about 300–400 μm thickness were cut using a diamond wire-saw. Next step was polishing the disks down to a thickness of about 80–120 μm using a lapping machine, on wet grinding paper. Then using a dimple-grinder, a sphere-shaped deepening was ground into the polished disk. Finally, the ion milling process was used to obtain TEM sample. Microscopic examination was per-formed at an accelerating voltage of 45 kV. The measurements of the hardness were done by means of a Shimadzu hardness tester (Vickers method). The microhardness within the processed zones was detected at the load of 0.981 N. A multiple load cycle with increasing load experiment was also done using nanoindenter Nan-oTest Vantage. This test was performed to determine the strain hardening and residual stress analysis of the processed steel. Minimum load was 500 mN and maximum load was 20 N. Loading and unloading rates were 50 mN/s. Indentation contains 7–10 cycles with 5 s dwell at maximum load. Phase identification of the modified layers was examined using X-ray diffractometry (XRD).

3. Results and discussion

The length of the pulses range from several dozens of microseconds to a hundred. Pulses produced luminescent plumes with the accompanying noise. The phenomenon was photographed with a high-speed camera, and selected images with characteristics time are presented in Fig. 1 (the relevant moments are described in successive photographs). The acquired images depict successive stages of generation, formation and disintegration of a luminescent plume at the beginning of the pulse. The acquired images present successive stages of generation and formation of a luminescent plume at the beginning of a pulse with the duration of 45 ms, repeated 50 times. As demonstrated in Fig. 1 (frames 453 and 454), a formed plume was registered in frame 454. The time of plume generation was 2 ms, and the total time of propagation until extinction, as shown in the successive images, was 12 ms, which accounted for only 4.4% of the time required to generate a single pulse. Plume size varied overtime, and this value was used to determine propagation velocity. Calculated speed of propagation velocity was 5.255 × 102cm/s. The time between plume generation and disappearance approximated 28% of pulse duration. The shape of the luminescent plume and the changes observed during its generation were very similar to those noted in interactions between a plasma stream and the surrounding gas (source: Institute of Plasma Physics and Laser Microfusion),which suggests that the analyzed object was a luminescent plasma plume. Converted energy of a laser pulse was estimated at 30 J. The time of luminescent plume generation suggests that laser plasma can be generated only by initial pulse energy. The generation process was repeated during successive

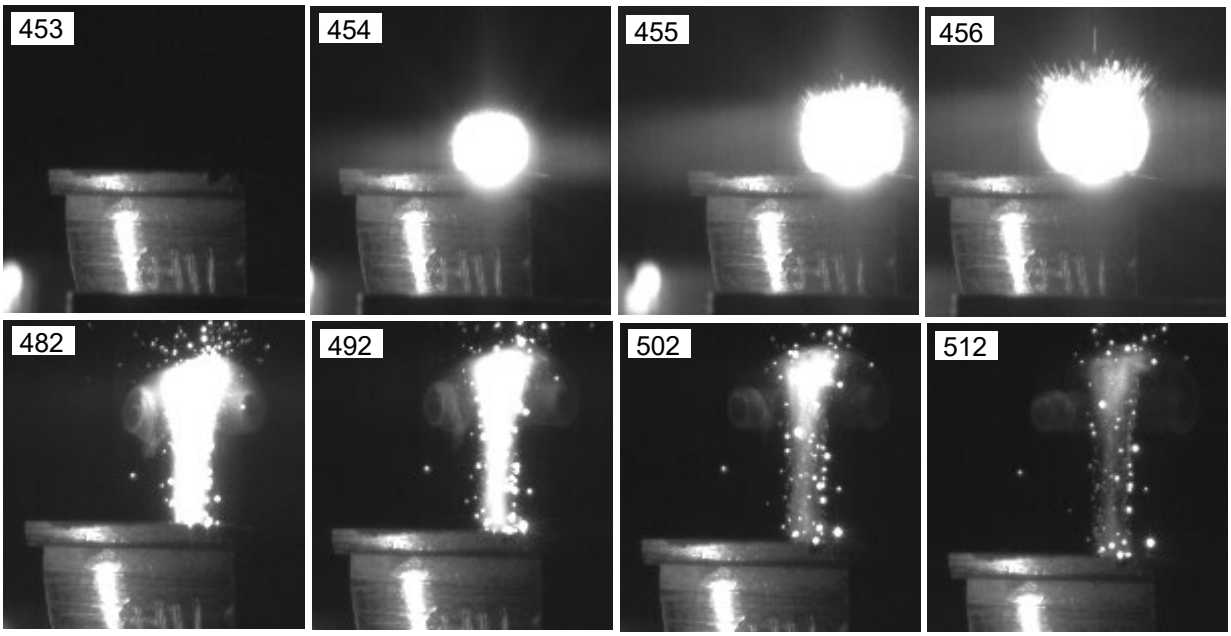

Fig. 1. Successive frames of a luminescent plume. The number displayed by each image is the frame number. Recorded every 0.222 ms. First frame – 453, successive frames– every 0.222 ms, followed by images acquired every 10 frames.

pulses. The above is consistent with the actual distribution of energy in a pulse produced by a carbon dioxide laser (Duley, 1976) where nearly the entire energy is concentrated at the beginning of the pulse generation process. The laser melted path is shown in Fig. 2. The melted path has characteristic “folds”, and it comprises a series of overlap-ping melted areas. Regardless of length of pulse, the

Fig. 2. Melted path produced by CO_2 laser beam and a luminescent plume formed on a sample of C80U steel in processing program 8, under 20× magnification, with a visible heat-affected zone (depicted by arrow).

resulting melted paths were characterized by “folds” whose sizes were varied depending on the parameters of the laser beam. In this experiment, the distance between “folds” approximated 0.45 mm. The distance between adjacent “folds” correlated with the beam displacement velocity and this correlation indicates that plumes were generated cyclically at the beginning of the generation of successive pulses. Long laser pulses (>50 ms) can lead to overheating of the processed surface and its evaporation. This may cause unevenness. To check if the surface roughness was the result of evaporation or due to the interaction of expended plasma with processed steel hardness testing was performed. The results of microhardness investigations are shown in Table 2. The range of the variation of microhardness varied depending on the place of measurement. Microhardness exceeded 3000 HV0.1 at “fold” peaks, which is characteristic of superhard materials. In samples of C80U steel, the above result could be the indicative of amorphicity or multiple material deformations. The microhardness of the analyzed material varied significantly between areas of measurement. The

Table 2
The results of microhardness investigations.

place the measurement of microhardness (see Fig. 3)							
Peak (1) 1.13 mm penetration into specimen surface		Rise (2) 0.9 mm penetration into specimen surface		Cavity (3) 0.97 mm penetration into specimen surface		Cavity (4) 0.62 mm penetration into specimen surface	
diagonal of indentation	$HV_{0.1}$	diagonal of indentation	$HV_{0.1}$	diagonal of indentation	$HV0_{.1}$	diagonal of indentation	$HV0_{.1}$
7.8	3048	7.5	3297	10.1	1818	10.0	1854
10.5	1682	18.6	536	14.5	882	22.1	379.7
21.3	408.7	19.1	513.7	20.9	424.5	22.4	372.9
21.1	416.5	22.1	379.7	23.9	324.6	—	—
22.3	372.9	—	—	—	—	—	—
the arithmetic mean	1185.6	the arithmetic mean	1181.6	the arithmetic mean	862.3	the arithmetic mean	868.9
the standard deviation	1055.5	the standard deviation	1222.8	the standard deviation	590.5	the standard deviation	696.6

above could point to varied impacts of energy and force at the place of measurement and different heat dissipation conditions. In selected measurement points, microhardness values reached 3200–3100 HV, 1800 HV and 400–300 HV at penetration depth of 1 mm in the peak area. Micro-hardness did not exceed 1854 HV in the cavities between “folds” (Fig. 3). The analyzed material crumbled on the surface, and no measurements were performed at the surface layer. Hardness of C80U steel after

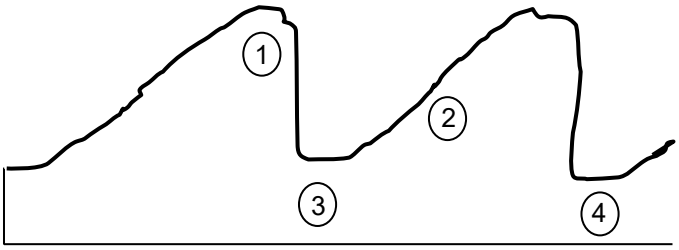

Fig. 3. Diagram showing the place in microhardness measurements on the longitudinal section of the melted path.

conventional, solid state hardening generally does not exceed 900 HV. Hardness about 2500 HV0.1 in some area melted by the pulsed laser beam, is achieved through a complex microstructure. XRD investigation and SAD analysis revealed the presence of martensite, cementite $(FeCrMn)_3C$ and small amount of retained austenite in microstructure (see Fig. 4). To explain such large differences in the values of hardness measurements, microscopic examination was performed. Microscopic

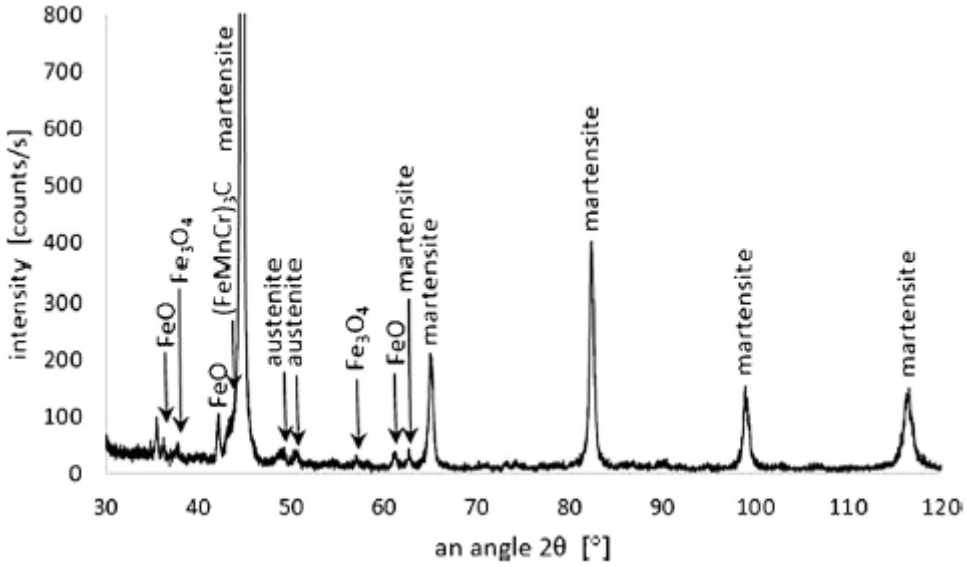

Fig. 4. XRD diffraction pattern of processed C80U steel.

examination revealed microstructure differences in the selected zones of melted path. In all investigated areas microstructure was composed of fine martensite, a small amount of retained austenite and partially dissolved cementite, but in the areas with greater hardness the observed martensite and retained austenite had much more crystallographic defects (see Figs. 5–8). The microstructure presented in Figs. 5 and 6 indicates that fine-plate martensite was formed under the high stress leading to the formation of twinned martensitic plates and Fig. 7 and Fig. 8b show martensite with a high density of crystallographic defects. Additionally, the expanding plasma cloud have generated impact and compressive stress in the processed steel which contributed to greater efficiency of austenite → martensite transformation. In high carbon steel conventional solid state hardening generates large amount of retained austenite inter alia due to the fact that the martensite finish temperature is lower than ambient temperature. Compressive stress due to expanding plasma facilitated the martensitic transformation thereby reducing the amount of retained austenite and increased hardness. In areas with lower hardness plates and needles of martensite were not so deformed (Fig. 8a) and the needles varied in size. In some areas there have been incomplete dissolved cementite next to the presence of martensite. The formation of such a microstructure may encourage very high heating rate, short pulse duration of repeated heat cycle, multiple austenite/martensite transformation and multiply repeated grains fragmentation. The temperature of the beginning of the austenitic transformation increases with an increase in the heating rate. Along with increasing temperature of austenitic transformation the number of crystal nuclei also increases. For example, during austenite transformation at 740 ^{o}C the number of crystal nuclei resulting from crystallization in 1 cm^3 in 1 s is 23 × 10^2, and at the temperature of 800 ^{o}C is 60 × 10^4 (Mirkin, 1975). The presumption is that in the conditions of the experiment being carried out in this work, the temperature of the beginning of the austenitic transformation was significantly greater than 800 ^{o}C what could be the cause of such a large fragmentation of austenite grains and very fine needles of martensite resulting from the rapid cooling. The short duration of the laser pulse and the total duration of the impact of the laser beam do not allow total dissolution of cementite. In turn, the rapid, periodically repeated heating and cooling of the area could have caused the martensite viewed in the microstructure, as the result of multiple phase transformation, passing along with a change of the temperature of the laser pulse. At the time of a pulse laser beam heating there were a few hundred pulses and a few hundred gaps between pulses, and so heating and cooling of the microareas occurred a few hundred times. As a result, in the following transformations austenite and martensite formed out of it were getting finer.

As a result, there occurs an increase of the amount of grain boundaries and thereby the increase of the density of crystal defects. Metallographic investigation using TEM revealed high density twins and dislocations in fine plates of martensite and in retained austenite. The specific volume of martensite, greater than the specific volume of austenite by about 3%, resulting in the residual stresses, could not be the sole cause of such dislocation structure, because the obtained microstructure strongly differs from the microstructure after conventional hardening. As far as fine plates of martensite can be explained by a very large number of crystal nuclei and high rate of austenite/martensite transformations, causes of a large number of twins and accumulations of dislocation within the martensite and retained austenite should be sought in other physical phenomena that may occur during the interaction of the laser beam with the processed material. Residual stresses due to a change in specific volume during phase transformation are not sufficient to induce such dislocation structure. There is a need of an external energy causing plastic strain of processed steel. Plastic strain can proceed as a deformation by twinning or by slip. Deformation by twinning occurs in the case of movement stoppage of dislocations. Under extreme conditions, such as shock-wave loading, the material deforms at very high strain rate and twinning may play an important role. From theoretical considerations, it appears that temperature-stress conditions of deformation mechanisms, including twinning, can occur at pressures of stress-inducing from 100 to 1000 MPa. Slip stoppage, in the case of our experience, could result from the pile-up of dislocations as a result of residual stresses caused by phase transformation and shock-wave loading due to pulsating plasma. The same effect also causes incomplete dissolving of cementite in martensitic and austenitic (retained austenite) matrix. Martensite and austenite twins can, however, be created when an external force reaches a sufficiently large value being able to induce the residual stresses between a few hundred and a thou-sand MPa. For the estimation of the residual stresses in melted material, and for comparison with the heat affected zone, hardness test was performed. A multiple load cycle with increasing load from 0.5 N to 20 N with 7–10 cycles was done. During indentation penetrator of a hardness tester performs the work needed for elastic and plastic deformation of the tested material. Work needed for elastic deformation can reflect the residual stress in investigated material. Fig. 9 shows the load curve as a function of the depth of the intender for the measurement in the heat affected zone and Fig. 10 shows the same relationship for a place in the melted path (No. 2 – see Fig. 3).These measurements were used to designate the percentage fraction of elastic work deformation during hardness test. Fig. 11presents the percentage fraction of elastic work as a function of depth. As can be seen from Fig. 11, the percentage fraction of elastic work for both heat affected zone and the melted material is the smallest for the first measurement (load of 0.5 N). This is particularly evident for melted material. This may result from the fact that brittle oxides formed on the surface of the melted material, while it was still hot. First measurement of hardness punctured surface oxides, therefore, portion of elastic work for this measurement is the smallest. The next measurement of hardness disclosed the largest percentage fraction of elastic work for melted steel that was 98.42% of total strain work. In the subsequent measurement, fraction of elastic work decreased and fluctuated within 89–91%. Such a diagram provides an occurrence of the presence of the biggest residual stresses near the surface and their reduction with the depth of melted steel. In turn the portion of elastic work strain shows little changes with the increase of the load for the measurement in the heat affected zone. The range of variability of elastic strain portion for this area is from 93.7 to 96.4%. Such a diagram provides almost the same residual stresses with the depth for the heat affected zone. The microstructure of the core material in the vicinity of the transition layer (shown in Fig. 5), is similar to the microstructure resulting from the process of plastic strain of steel at elevated

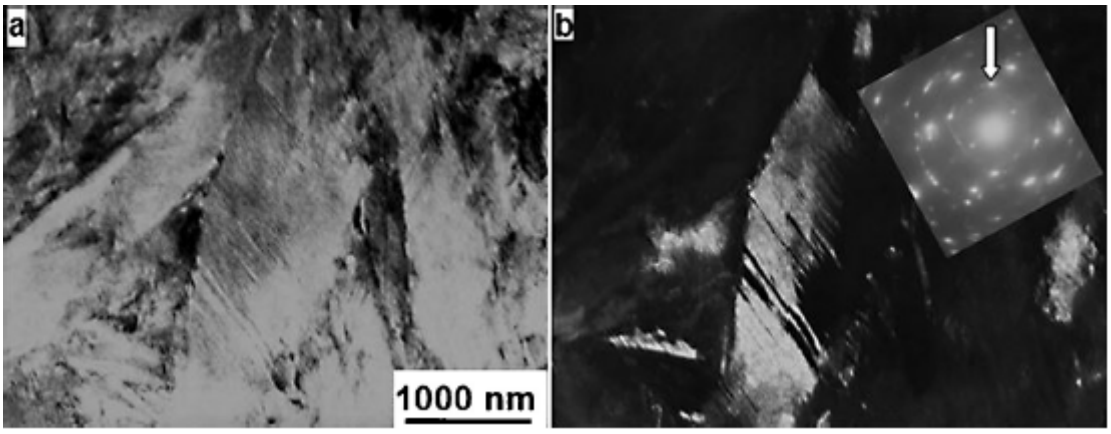

Fig. 5. TEM images in bright (a) and dark (b) field, made in the selected diffraction reflex (depicted by arrow) showing microtwins in martensitic plates – rise.

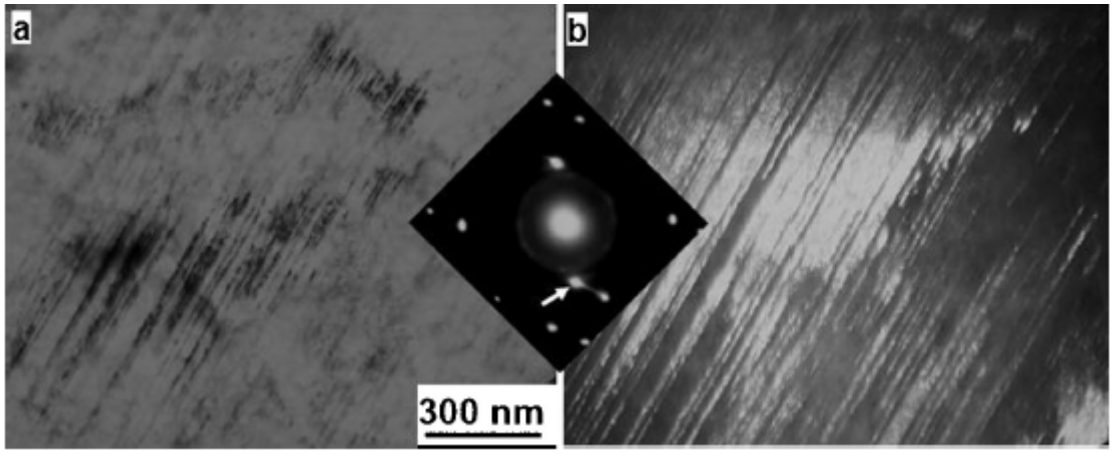

Fig. 6. TEM images in bright (a) and dark (b) field, made in the selected diffraction reflex (depicted by arrow) showing microtwins in martensitic plate – peak.

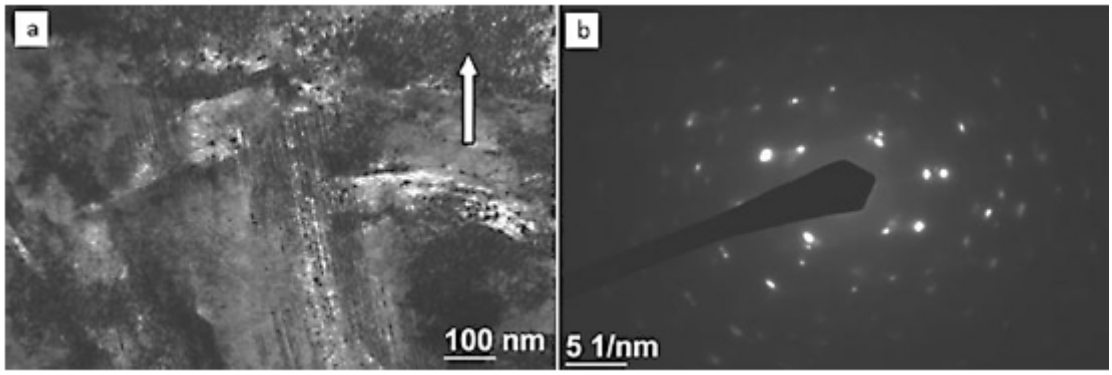

Fig. 7. A high density of crystallographic defects in a martensite. Strong dislocation scattering of an electron beam is depicted by arrow. TEM image in bright field (a) and the corresponding diffraction pattern (b) – peak.

temperatures. The microstructure is akin to dislocation structures of subgrains, which are created in dynamic recovery process during plastic strain above the recrystallization temperature. Created dislocation structure inhibits the process dynamic recovery which leads to gaining the balance between the strain hardening and dynamic recovery processes which removes that strengthening. Achieving this balance shall be subject to the condition of the steady plastic flow, which occurs with

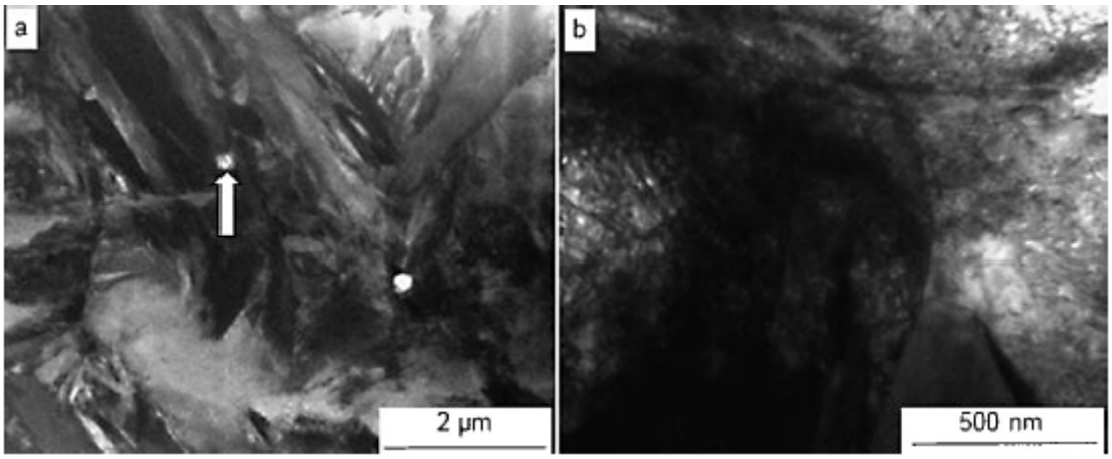

Fig. 8. Incomplete dissolved cementite in the martensitic matrix (depicted by arrow) visible in bright field – cavity (a) and a high density of dislocations in a martensite (b)– rise (TEM).

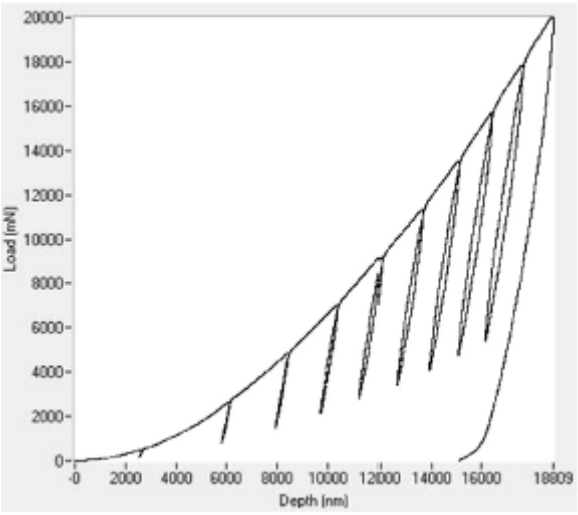

Fig. 9. Load vs. depth of indenter for heat affected zone.

specific values of plastic strain. In the case of a significant plastic deformation, above the recrystallization temperature, there is a dynamic recovery during plastic deformation process, as far as the degree of cold work (even locally), exceeds the value of critical dynamic recrystallization strain ε_{crd}. New grains, created as a result of the front passage of a dynamic recovery, saturate dislocations again in the next stage of plastic deformation. Depending on the rate of strain, recovery may be periodic or continuous. One should believe that laser processing parameters at which this microstructure resulted, have to cause the occurrence of conditions, which have reached the steady plastic flow. In turn, depending on the rate of strain, recovery and steady plastic flow could have the dual nature. In the case where critical dynamic recrystallization strain ε_{crd} is greater than strain required for recovery overwhelming the volume of deformed metal ε_{rpo}, one cycle of recrystallization is completed prior to the start of the next – resulting in a curve of strain hardening showing the oscillations, and dynamic recovery is periodic. But when $\varepsilon_{rpo} > \varepsilon_{crd}$, one wave of recrystallization does not have time to go through the deformed steel, and the second one starts, strain hardening curve is smooth, and recovery-continuous. The microstructure was created as a result of the cyclical impact of laser pulses, which generated shock waves. Shock waves displace into the processed material dissipating their energy, causing the formation of twins and dislocations. In this case strain hardening has the largest value on the surface of the processed material, and decreases with depth. Fig. 12 presents the changes in hardness with the depth of the material for melted steel and for heat

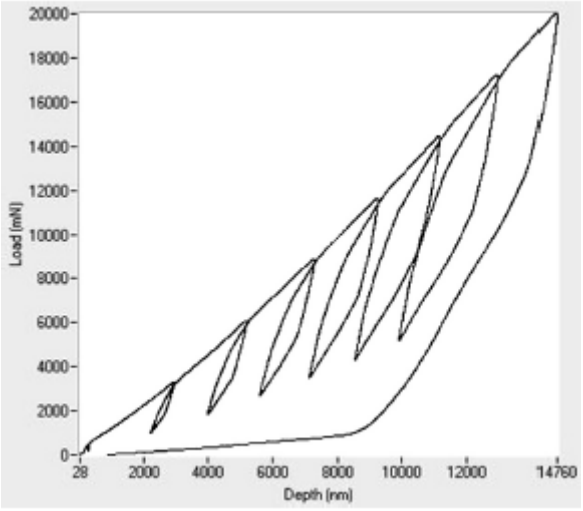

Fig. 10. Load vs. depth of indenter for melted steel.

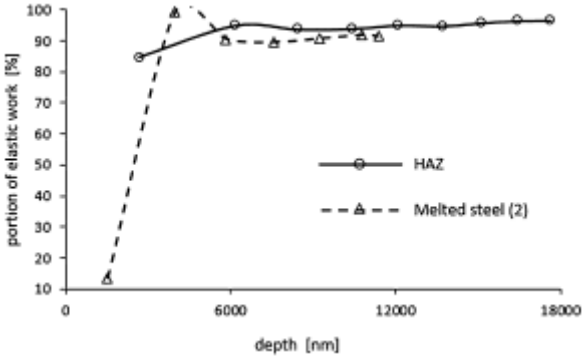

Fig. 11. Percentage portion of elastic work for heat affected zone and for melted steel.

affected zone. As can be seen in Fig. 12 the maximum hardness of melted steel (place No 2) is 13.16 GPa. It occurs at the surface and decreases with a depth. At the depth of11.7 μm the hardness of processed steel is only 5.09 GPa. Another hardness profile is observed for the heat affected zone. Hardness profile for this area is flat and shows no major changes at a depth of hardened steel.

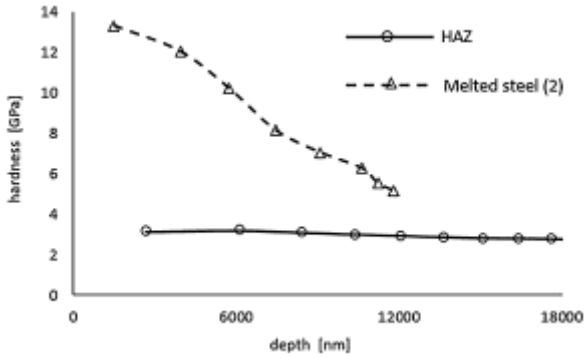

Fig. 12. Hardness profiles for heat affected zone and for melted path (place No 2).

4. Conclusions

The results of this study allow to draw the following conclusions:

– long pulses generated by a CO_2 laser, affecting a carbon C80U steel sample placed between two permanent magnets, may produce a plasma plume,

– melting of C80U steel using optical discharge plasma allows to obtain microstructure consisting of highly defected fine-plate martensite with a certain number of incompletely dissolved cementite and a small amount of retained austenite,

– shock waves formed as a result of plasma plume propagation interact with the melted steel, thus contributing to the strain hardening of processed material,

– heating C80U steel by a series of long laser pulses generated by a CO_2 laser, causes a large residual stresses at the surface of the processed material,

– high defects density of crystal lattice caused by the strong fragmentation of the microstructure and plastic deformation during laser melting are major reasons for the increase of the hardness of the processed steel. Surface hardness values for this kind of microstructure are very high and atypical in comparison with the hardness values for high-carbon steel hardened via solid-state phase transformation.

The results point to the possibility of using CO_2 laser beam to modify the top layer of high carbon steel and obtain much higher hardness than the one obtained ordinary laser surface melting.

Acknowledgements

The authors would like to thank Professor Jan Kusiński, PhD,Eng., from the AGH University of Science and Technology in Cracow, for his help in microstructure interpretations.

References

Basu, A., Samant, A.N., Harimkar, S.P., Dutta Majumdar, J., Manna, I., Dahotre, N.B.,2008. Laser surface coating of Fe–Cr–Mo–Y–B–C bulk metallic glass composition on AISI 4140 steel. Surf. Coat. Technol. 202, 2623–2631.

Bień, A., Szachnowski, W., 1996. Optimisation of laser modified surface layer homogeneity. In: Wolinski, W., Kusinski, J. (Eds.), Proceedings of the Society of Photo-Optical Instrumentation Engineers (SPIE). Szczecin Świnoujscie, Poland, pp. 48–54.

Breczko, T., Bień, A., 2006. Influence of multiple melting on the structure and geometry of the surface layer of 50H steel. In: Melker, A.I. (Ed.), Proceedings of the Society of Photo-Optical Instrumentation Engineers (SPIE). St. Petersburg, Russia, p. E2530.

Duley, W.W., 1976. CO2Laser-effects and Applications. Academic Press, New York.

Dutta Majumdar, J., Galun, R., Mordike, B.L., Manna, I., 2003. Effect of laser surface melting on corrosion and wear resistance of a commercial magnesium alloy. Mater. Sci. Eng. A361, 119–129.

Gireń, B.G., Szkodo, M., Steller, J., 1999. The influence of residual stresses on cavi-tation resistance of metals – analysis based on investigations involving metals remelted by a laser beam and optical discharge plasma. Wear 233–235, 86–92.

Institute of Plasma Physics and Laser Microfusion: Study and applications of Laser – Master interaction at low laser intensities, 2012. www.fusenet.eu/member/82

Jiang, J., Xue, L., Wang, S., 2011. Discrete laser spot transformation hardening of AISIO1 tool steel using pulsed Nd:YAG laser. Surf. Coat. Technol. 205, 5156–5164.

Kac, S., Kusiński, J., 2004. SEM structure and properties of ASP2060 steel after laser melting. Surf. Coat. Technol. 180–181, 611–615.

Mirkin, L.I., 1975. Physical Basis of Material Processing by Laser Beam. Izd. MGU, Moscow (in Russian).

Nath, A.K., Gupta, A., Benny, F., 2012. Theoretical and experimental study on laser surface hardening by repetitive laser pulses. Surf. Coat. Technol. 206, 2602–2615.

Szkodo, M., 2005. Relationship between microstructure of laser alloyed C45 steel and its cavitation resistance. J. Mater. Process. Technol. 162–163, 410–415.

Telasang, G., Dutta Majumdar, J., Padmanabham, G., Manna, I., 2014. Structure–property correlation in laser surface treated AISI H13 tool steel for improved mechanical properties. Mater. Sci. Eng. A599, 255–267.

Yasavola, N., Abdollah-zadeha, A., Ganjalib, M., Alidokhta, S.A., 2013. Microstructure and mechanical behavior of pulsed laser surface melted AISI D2 cold work tool steel. Appl. Surf. Sci. 265, 653–662.